The Astrophysical Journal, 718:1–10, 2010 July 20 doi:10.1088/0004-637X/718/1/1

SPITZER OBSERVATIONS OF BLACK HOLE LOW-MASS X-RAY BINARIES: ASSESSING THE NON-STELLAR INFRARED COMPONENT

Dawn M. Gelino[1], Christopher R. Gelino[2], and Thomas E. Harrison[3]
[1] NASA Exoplanet Science Institute, California Institute of Technology, Pasadena, CA 91125, USA; dawn@ipac.caltech.edu
[2] Infrared Processing and Analysis Center, California Institute of Technology, Pasadena, CA 91125, USA
[3] New Mexico State University, Las Cruces, NM 88003, USA
Received 2009 July 17; accepted 2010 May 15; published 2010 June 24

ABSTRACT

We have combined ground-based optical and near-infrared data with *Spitzer Space Telescope* mid-infrared data for five black hole (BH) soft X-ray transients (SXTs) in order to determine the levels of near- and mid-infrared emission from sources other than the secondary star. Mid-infrared emission from an accretion disk, circumbinary dust, and/or a jet could act as sources of near-infrared contamination, thereby diluting ellipsoidal variations of the secondary star and affecting determined BH mass estimates. Based on optical to mid-infrared spectral energy distribution modeling of the five SXTs along with the prototype, V616 Mon, we detected mid-infrared excesses in half of the systems, and suggest that the excesses detected from these systems arise from non-thermal synchrotron jets rather than circumbinary dust disks.

Key words: accretion, accretion disks – binaries: close – binaries: symbiotic – infrared: stars – stars: late-type – X-rays: binaries

Online-only material: color figure

1. INTRODUCTION

Soft X-ray transients (SXTs) are a class of low-mass X-ray binaries (LMXBs) that exhibit large and abrupt X-ray and optical outbursts that can be separated by decades of quiescence. The compact object in these systems is either a black hole (BH) or a neutron star (NS) and the companion/secondary star is a low-mass K- or M-type star (see Charles & Coe 2006 for a review). During outburst, the optical spectrum is flat while the light curve follows a fast rise exponential decay (FRED) behavior where the system brightens dramatically over a few days and decays back to its quiescent value, occasionally exhibiting additional smaller maxima along the way. The outbursts are the result of a sudden, significant increase in the rate of mass accretion onto the compact object due to a temperature–opacity instability in the accretion disk (Cannizzo 2000; Lasota 2008).

As evidenced by Doppler tomography of emission lines and optical variability, accretion disks are still present when the systems are in their quiescent states. Despite this, quiescent BH SXTs are very faint at X-ray, optical, and infrared (IR) wavelengths. While the quiescent X-ray emission can be caused by accretion onto a compact object (Garcia et al. 2001; Wijnands 2005), the Roche lobe-filling companion can dominate the luminosity at optical and IR energies (however, see Bildsten & Rutledge 2000). During the binary orbit, the changing aspect of the tidally distorted companion causes a periodic modulation of the optical and IR emission (Gelino 2001). Measurements of these "ellipsoidal variations" provide information about the physical parameters of the binary.

In order to determine the mass of a BH or NS in an LMXB, the orbital inclination angle (i), orbital period, amplitude of the radial velocity curve, and mass ratio of the two components must be known. The inclination angle is the most difficult parameter to measure, and in most cases is the leading uncertainty in the derivation of the compact object mass. Since most LMXBs are non-eclipsing, modeling the ellipsoidal variations of the secondary star is currently the favored method to accurately determine the orbital inclination. The amplitude of the ellipsoidal variations is sensitive to i; however, this amplitude can be affected not only by the orbital inclination, but also by other light sources in the system. For example, if there is significant emission from the accretion disk at the observed wavelength, then this light will dilute the ellipsoidal variations and simulate a system of lower inclination. Possible sources of "contaminating" flux include the accretion disk, accretion hot spots, circumbinary dust, and synchrotron emission from jets.

Recent models have predicted that since BH SXT accretion disks have a large projected surface area compared to that of the companion, a cool (∼3000 K), optically thick disk may produce a significant contribution to the IR while remaining difficult to detect in the optical (Hynes et al. 2005). Since this disk material would be distributed in an axisymmetric fashion, it would act as a near-constant source of diluting light and would not distort the near-IR (NIR) light curves. Previous dilution estimates based on measurements of emission lines in the spectrum of the prototype BH SXT, V616 Mon (A0620-00), gave an upper limit to the disk light in the system of 27% in the R band (Shahbaz et al. 2003). However, Harrison et al. (2007) found little evidence of any such emission based on the Keck II NIRSPEC K-band spectra of this source. Cantrell et al. (2010) in fact find that dilution estimates were not properly constrained in the past, and when combined with unrecognized state changes and intrinsically changing light curve shapes, can account for disagreements on the inclination of V616 Mon.

The predicted spectral energy distributions (SEDs) of quiescent accretion disks are expected to be flatter than the Rayleigh–Jeans tail of the cool secondary star SED. Thus, if flux from the disk is a significant component of the near-infrared luminosity, it can become dominant at longer wavelengths. Due to its shallow spectral slope, the most difficult contamination source to extract in many BH SXT light curves is one produced by free–free emission. However, if this free–free emission were a significant component of the optical/NIR luminosity, it will be easily detected in the mid-IR. Thus, to completely account for

Table 1
SXT Properties

Target	X-ray Name	P_{orb} (hr)	Sp T_2	a ($R_\odot$)	i (°)	M_1 ($R_\odot$)	Distance (kpc)
V518 Per[a]	GRO J0422+32	5.09	M1	2.45 ± 0.24	45 ± 2	3.97 ± 0.95	2.49 ± 0.30
MM Vel[b]	GRS 1009-45	6.85	M3	2.93 ± 0.13	58 ± 4	5.27 ± 0.60	3.82 ± 0.27
QZ Vul[c]	GS 2000+25	8.26	K5	4.14 ± 0.13	64 ± 2	7.70 ± 0.66	2.29 ± 0.15
V406 Vul[d]	XTE J1859+22	9.16	K0	...	"high"	> 6.3	8 ± 3
GU Mus[e]	GS 1124-68	10.38	K4	4.85 ± 0.15	54 ± 2	7.24 ± 0.70	5.89 ± 0.26

Notes.
[a] Gelino & Harrison (2003) and references therein.
[b] This paper and Gelino (2002) and references therein.
[c] Gelino (2001) and references therein.
[d] Zurita et al. (2002) and references therein.
[e] Gelino et al. (2001a) and references therein.

the amount of NIR contamination in the ellipsoidal light curves, we need to accurately characterize the optical/IR SEDs of these systems.

While emission from the accretion disk is expected to be the main culprit for contaminating the NIR light, emission from circumbinary material might dominate the mid-IR SEDs of BH SXTs. Muno & Mauerhan (2006) observed excess emission in *Spitzer* IRAC 4.5 and 8.0 μm and MIPS 24 μm data from three BH LMXBs: V616 Mon, V404 Cyg (GS 2023+33), and KV Uma (XTE J1118+48). The excesses in two of these systems were interpreted as originating from cool, circumbinary material. Gallo et al. (2007), however, argue that their composite radio/IR/optical spectra of the same targets did not require circumbinary dust emission, even though they could not rule out its presence. Gallo et al. (2007) further suggest that a significant fraction, if not all, of the mid-IR excess emission in these systems could be accounted for by non-thermal emission from a jet.

The presence of synchrotron emission from these systems during outburst was first suggested by Owen et al. (1976) for V616 Mon, and later confirmed by Hjellming et al. (1998) for QZ Vul (GS 2000+25). Hjellming & Rupen (1995) linked the relativistic jets of GRO J1655-50, SS433, and GRS 1915+105 to radio flares in V616 Mon, QZ Vul, V404 Cyg, and GU Mus (GS 1124-68). Indeed, from optical/NIR/X-ray observations of 33 X-ray binaries, Russell et al. (2006) found that while X-ray reprocessing of disk light is the main mechanism responsible for optical-IR emission when a BH SXT is in the soft (bright) state, synchrotron emission from jets is the main source of NIR light when the systems are in the hard (low) state. Furthermore, they show that the radio–NIR jet spectrum in BH SXTs is basically flat for a given X-ray luminosity, and that the optically thick–optically thin turnover in the jet spectrum is likely to be close to the *K* band. In addition, Migliari et al. (2006) used *Spitzer* IRAC observations of the LMXB 4U 0614+091 to detect non-thermal emission from a compact jet ($F_\nu \sim \nu^\alpha$, where $\alpha = -0.57 \pm 0.04$).

All of these studies show that mid-IR emission sources could contaminate ellipsoidal light curves of BH SXTs. In order to help address the contamination issue, we have observed five BH SXT systems: QZ Vul, V518 Per, V406 Vul, GU Mus, and MM Vel (see Table 1 for properties of these systems) at mid-IR wavelengths with the IRAC camera on the *Spitzer Space Telescope*. We combine these data with ground-based optical and NIR photometry to create optical to mid-IR SEDs of each of the systems. In Section 2, we describe our observations and data reduction process. We describe the modeling and results for each of the five systems in Section 3. Finally, we discuss the implications of these models in Section 4.

2. OBSERVATIONS AND DATA REDUCTION

In this paper, we combine space-based, *Spitzer Space Telescope* data with ground-based optical and NIR data obtained from several different telescopes. We describe these observations and our data reduction process below.

2.1. Spitzer Space Telescope

Infrared observations were obtained using the IRAC instrument (Fazio et al. 2004) aboard the *Spitzer Space Telescope* (Werner et al. 2004) as part of General Observer program 40948 (PI: D. Gelino). We obtained images in all four IRAC channels centered at 3.6, 4.5, 5.8, and 8.0 μm. The exposure time for all images was 100 s. We used a nine position medium dither pattern. Given the expected faintness of the BH SXTs at IRAC wavelengths, we offset the targets 10″ from the center of the array in order to lower the probability of landing on a latent image from previous exposures of much brighter targets. The observing log is presented in Table 2.

The data were reduced using the MOPEX software package[4] distributed by the Spitzer Science Center. Reduction started with the basic calibrated data (BCDs) as produced by the IRAC pipeline. BCDs from versions S17.0.0 and later are corrected for several image artifacts, including banding and column pull down. Our data contain BCDs from both pre- and post-S17 pipelines (see Table 2) and our S16.1.0 data clearly exhibited banding and column pull down. Even though we were only concerned about a single point source near the center of the array, our targets were faint and so we corrected for these image artifacts using the artifact mitigation suite written by S. Carey.[5] We then combined all BCDs for a given target to create a final mosaic.

Photometry for our targets were obtained using the point response function (PRF) fitting routines in the APEX Multiframe package in the MOPEX distribution. We followed the prescription for IRAC point-source photometry detailed at http://ssc.spitzer.caltech.edu/irac/iracinstrumenthandbook/102/. In short, we searched for point sources in the final mosaics, and obtained the PRF fitting photometry on those detected sources in the individual BCDs. The fluxes from the individual BCDs were then averaged to form a final measurement for each source.

[4] http://ssc.spitzer.caltech.edu/postbcd/mopex.html
[5] http://spider.ipac.caltech.edu/staff/carey/irac_artifacts/index.html

Table 2
Spitzer IRAC Observing Log

Target	Field of View	Date (UT)	UT Start	UT End	AOR Key	Pipeline Version
V518 Per	[3.6] & [5.8]	2007 Oct 17	20:55:23.659	21:11:36.053	23365888	S16.1.0
	[4.5] & [8.0]	2007 Oct 17	20:38:48.766	20:55:03.659		
QZ Vul	[3.6] & [5.8]	2007 Oct 21	09:02:41.754	09:17:56.550	23365632	S16.1.0
	[4.5] & [8.0]	2007 Oct 21	08:46:07.333	09:02:22.957		
V406 Vul	[3.6] & [5.8]	2007 Oct 21	09:38:29.728	09:54:43.715	23365120	S16.1.0
	[4.5] & [8.0]	2007 Oct 21	09:21:56.877	09:38:11.728		
GU Mus	[3.6] & [5.8]	2008 Apr 8	09:47:57.287	10:04:11.668	23365376	S17.2.0
	[4.5] & [8.0]	2008 Apr 8	09:31:24.448	09:45:51.693		
MM Vel	[3.6] & [5.8]	2008 Jun 13	22:31:48.828	22:48:03.624	23364864	S18.1.0
	[4.5] & [8.0]	2008 Jun 13	22:15:15.149	22:31:30.437		

Table 3
Spitzer IRAC Fluxes

Target	[3.6] (μJy)	[4.5] (μJy)	[5.8] (μJy)	[8.0] (μJy)
V406 Vul	22.43 ± 0.55	16.15 ± 0.69[a]	2.86 ± 2.62[a]	< 4.0
V518 Per	47.74 ± 0.56	42.49 ± 0.80	37.72 ± 3.20	39.84 ± 4.60
QZ Vul	71.64 ± 0.93[a]	51.00 ± 0.88	29.99 ± 3.25[a]	25.30 ± 5.62[a]
GU Mus	92.18 ± 1.04[a]	80.70 ± 0.89	50.61 ± 2.16	36.74 ± 4.02
MM Vel	138.00 ± 0.98	88.60 ± 0.84	65.58 ± 2.09	37.75 ± 3.86

Note. [a] These fluxes are derived from the APEX QA residual images.

In 70% of our images, the targets were detected with the PRF routine on the first pass. For the images in which the target was not detected, we subtracted all of the point sources from the first pass BCDs (using APEX QA Multiframe) and then used APEX Multiframe to find point sources in the residual images. Since the residual images only have the point sources detected in the initial pass removed, the fluxes of any remaining sources are conserved. The final fluxes are presented in Table 3.

2.2. Palomar 200 Inch Hale Telescope

Near-infrared images of V406 Vul, V518 Per, and QZ Vul were obtained using the Wide-Field Infrared Camera (WIRC; Wilson et al. 2003) on the 200 inch Hale Telescope at Palomar Observatory over various nights from 2006 August to 2008 May. The observing log is presented in Table 4. For three of the SXTs, the ground-based Palomar data were obtained within one to three days of the IRAC data. WIRC has a pixel scale of 0.″25/pixel and a total field of view of 8.′7. Images were obtained in the J, H, and K_s filters. Conditions were photometric on all nights.

Images were reduced using a suite of IRAF scripts and FORTRAN programs kindly provided by T. Jarrett. These scripts first linearize and dark subtract the images. From the list of input images, a sky frame and flat-field image are created and subtracted from, and divided into (respectively), each input image. At this stage, WIRC images still contain a significant bias that is not removed by the flat field. Comparison of Two Micron All Sky Survey (2MASS) and WIRC photometric differences across the array shows that this flux bias has a level of ≈10% and the pattern is roughly the same for all filters. Using these 2MASS–WIRC differences for many fields, we can create a flux bias correction image that can be applied to each of the "reduced" images. Finally, we astrometrically calibrated the images using 2MASS stars in the field. The images were then mosaicked together and the mosaic was photometrically calibrated using 2MASS stars. Magnitudes were computed using the IRAF *phot* routine with the zero points found using the 2MASS stars.

2.3. Other Facilities

In order to create the optical to mid-IR SEDs of each of the five SXTs, we also obtained data from the Astophysical Research Consortium 3.5 m telescope at the Apache Point Observatory (APO) as well as the 0.9 m and Victor M. Blanco 4 m telescopes at the Cerro Tololo Inter-American Observatory (CTIO). All of these data have already been described and published in Gelino (2001, QZ Vul; APO), Gelino et al. (2001a, GU Mus; CTIO 4m and 0.9m), Gelino (2002, MM Vel; CTIO 4m), and Gelino & Harrison (2003, V518 Per; APO). These data sets are also described briefly in the relevant sections below.

3. RESULTS

We summarize the main properties of the program BH SXTs in Table 1. All of the systems were observed long after their last outburst and their *Rossi X-Ray Timing Explorer* All Sky Monitor (*RXTE* ASM) light curves[6] showed no sign of activity above normal levels at the epoch of the *Spitzer* observations. We now discuss each of the five SXTs in turn.

3.1. QZ Vul

QZ Vul was discovered on 1988 April 23 with the ASM aboard the *Ginga* satellite (Makino et al. 1988). The source attained maximum light on April 28 with a 1–6 keV flux of 12 Crab and decreased exponentially until the end of June and then underwent a "secondary maximum" in July before declining to its quiescent state. The optical counterpart was identified through the comparison of optical spectra and radio

[6] http://xte.mit.edu/asmlc/ASM.html

Table 4
Near-IR Observing Log

Target	Filter	Date (UT)	UT Start	UT End	Total Exp. Time (s)	Magnitude
V518 Per	J	2007 Oct 20	12:02:26.633	12:08:59.664	300	18.90 ± 0.07
		2008 Jan 26	05:37:57.522	05:44:38.342	300	18.98 ± 0.10
	H	2007 Oct 20	11:52:57.676	11:57:00.774	150	17.96 ± 0.10
		2008 Jan 26	05:23:42.273	05:27:04.332	100	18.11 ± 0.14
	K_s	2007 Oct 20	12:11:09.633	12:16:04.787	150	17.67 ± 0.14
		2008 Jan 26	05:31:11.216	05:34:32.226	100	17.83 ± 0.18
QZ Vul	J	2007 Oct 20	03:08:43.679	03:15:16.739	300	17.89 ± 0.04
		2008 May 09	12:10:01.267	12:16:28.918	300	17.66 ± 0.08
	H	2007 Oct 20	03:17:44.637	03:21:47.845	150	17.04 ± 0.04
		2008 May 09	12:18:51.850	12:22:48.954	150	16.92 ± 0.05
	K_s	2007 Oct 20	03:23:24.688	03:26:46.276	100	16.74 ± 0.08
		2008 May 09	12:24:26.867	12:28:02.025	100	16.77 ± 0.09
V406 Vul	J	2007 Oct 20	02:43:03.678	02:47:06.676	150	19.50 ± 0.17
		2006 Aug 14	04:07:48.892	07:41:46.054	5040	19.95 ± 0.04
		2006 Aug 15	05:28:20.980	09:47:21.955	13440	20.06 ± 0.03
		2006 Aug 16	03:22:28.886	05:33:50.043	6480	20.06 ± 0.04
	H	2007 Oct 20	02:36:00.543	02:40:03.740	150	19.01 ± 0.16
		2006 Aug 14	05:41:52.419	06:37:14.795	2280	19.29 ± 0.05
		2006 Aug 16	05:39:52.023	08:29:05.038	5040	19.15 ± 0.04
		2006 Aug 17	04:03:48.979	09:13:39.966	13440	19.17 ± 0.02
	K_s	2006 Oct 20	02:51:04.930	02:55:59.875	150	19.09 ± 0.35
		2006 Aug 14	06:47:13.060	07:06:34.031	700	18.49 ± 0.24
		2006 Aug 15	04:11:06.083	05:14:37.034	2400	19.01 ± 0.11
		2006 Aug 16	08:33:51.962	09:15:49.001	1680	18.78 ± 0.12

measurements to those of V616 Mon (Tsunemi et al. 1989). At the peak of its optical outburst, QZ Vul reached $V = 16.4$ mag, an increase of only 4.8 mag from its quiescent value (Charles et al. 1991), to which it returned in about one year.

Figure 1 presents the optical to mid-IR SED for QZ Vul. Gelino (2001) estimated the extinction to be $A_v = 4.05$ for this source. We find a slightly lower value of the extinction, $A_v = 3.8$, and the filled circles represent the observed data dereddened by this amount, including the IRAC data using the extinction relations listed in Flaherty et al. (2007). The open stars represent the SED of a K2V. While the IRAC and *JHK* data were taken only one day apart, the optical data were obtained in 2001 with SPIcam[7] on the Astrophysical Research Consortium 3.5 m telescope at APO. The K2V SED is consistent with the observed data set and indicates no excess NIR or mid-IR emission.

3.2. V406 Vul

V406 Vul was discovered by Wood et al. (1999) using the *RXTE* ASM in October 1999 and the optical counterpart was quickly identified by Garnavich & Quinn (2000). The system behaved like a typical SXT during outburst in both the X-ray and optical regimes. Since outburst, there have not been many studies of this system despite it having the largest apparent mass function of the LMXB class, $f(M) = 7.4 \pm 1.1\ M_\odot$ (Filippenko & Chornock 2001). Based on observations taken prior to, and during quiescence, Zurita et al. (2002) state that the inclination angle of this distant SXT must be "high." The existing data set for this system is limited, with no published attempts to search for IR ellipsoidal variations. However, an NIR ellipsoidal study is currently underway on the Palomar 200 inch telescope D. Gelino & C. Gelino (2010, in preparation). A *J*-band finder chart for V406 Vul is presented in Figure 2. This image is the sum of roughly 6 hr of data taken with WIRC. The gradient seen in the background of the image is due to a $J = 7.4$ mag star (HD 343516) located 82″ south of V406 Vul. We have dereddened the photometry by $A_V = 1.8$ mag, with this reddening estimated using the "Galactic Dust Reddening and Extinction" calculator (at http://irsa.ipac.caltech.edu/applications/DUST/). The resulting SED is shown in Figure 3. The open stars represent

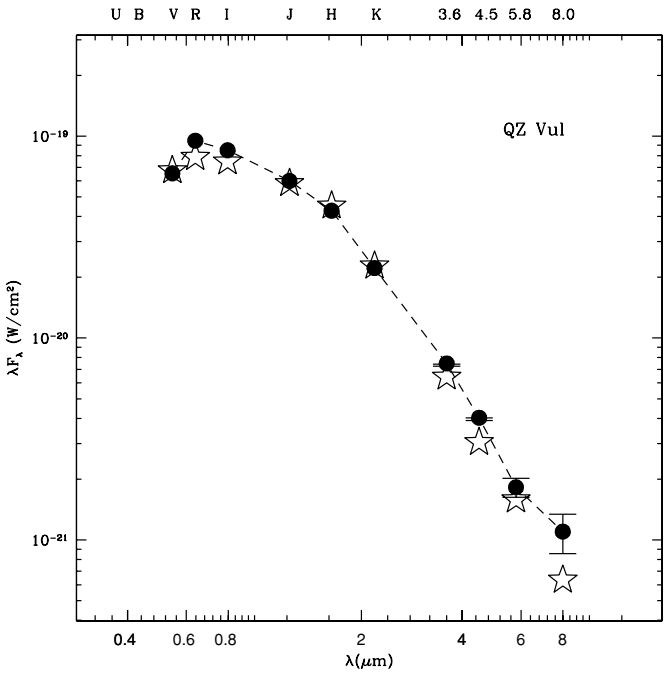

Figure 1. Optical to mid-IR SED for QZ Vul (filled circles). The photometry has been dereddened by $A_V = 3.8$ mag. Error bars are 1σ and are much smaller than the points when not shown. The observed SED is compared with the SED of a K2V (open stars). The two SEDs match well within the errors, indicating no detected NIR or mid-IR excess emission.

[7] http://www.apo.nmsu.edu/arc35m/Instruments/SPICAM/

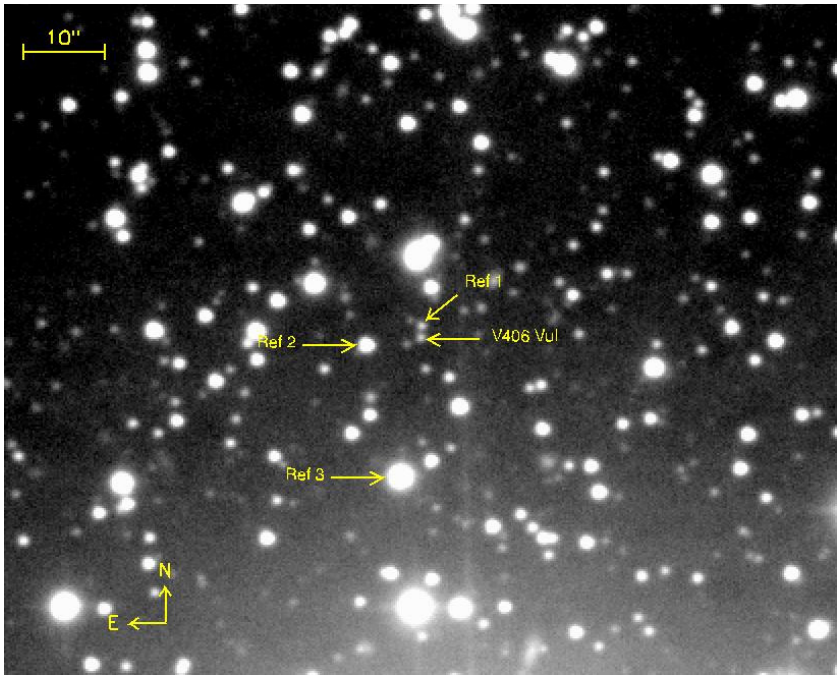

Figure 2. *J*-band finder chart for V406 Vul from the Palomar 200 inch telescope. The image is the sum of roughly 6 hr of data. The background variation is due to a bright star just off the bottom of the image.
(A color version of this figure is available in the online journal.)

an M3V (with $T_{BB} \sim 3300$K). The filled circles are the observed SED of V406 Vul. The optical (*V* and *R*) points were obtained in 1999 by Zurita et al. (2002). The NIR data were obtained on 2007 October 21, one day after the *Spitzer* observations. The arrows indicate 3σ upper limits to the IRAC fluxes. Note the star 1.″4 north of the system in Figure 2. This star is resolved from V406 Vul in the ground-based data, but cannot be separated in the IRAC data due to the large pixels of the IRAC imager. The optical and NIR magnitudes of these two stars are presented in Table 5. The observed optical/NIR SED of V406 Vul is well fit by the M3V SED. This spectral type is in contrast with previous estimates of the secondary star spectral types of late G/early K (Zurita et al. 2002), but the extinction remains poorly constrained. The nearby field star ("Ref 1") has similar optical and NIR colors and fluxes to V406 Vul, and the observed IRAC points are consistent with the sum of the two sources. Based on these arguments, we conclude that V406 Vul does not possess a significant mid-IR excess.

3.3. MM Vel

MM Vel was discovered by both the *GRANAT* (Lapshov et al. 1993) and *Compton Gamma Ray Observatory* satellites (Harmon et al. 1993) on 1993 September 12. The outburst X-ray spectrum was modeled with a 0.5 keV soft component and a power law with spectral index of -2.5 in the 10–100 keV energy range (Kaniovsky et al. 1993). The optical counterpart was discovered on 1993 November 17 by Della Valle & Benetti (1993). The optical outburst light curve was similar to that of V518 Per (GRO J0422+32) with a secondary optical outburst and various mini outbursts (Callanan et al. 1995). The faint optical counterpart is extremely close (<1.″5) to a $V = 17.9$ mag late-G star (Masetti 1997), making optical and infrared observations difficult (see Della Valle et al. 1997 and Shahbaz et al. 1996 for finder charts).

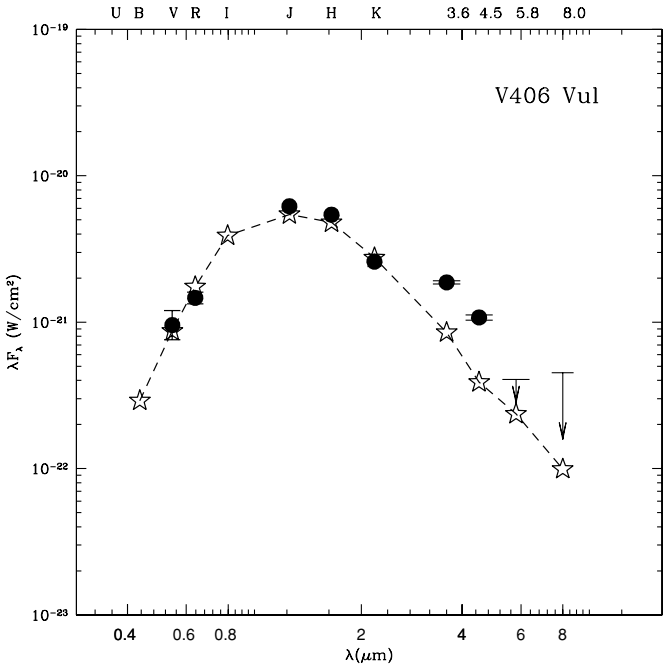

Figure 3. Optical to mid-IR SED for V406 Vul (filled circles). The optical and NIR (*VRJHK*) data have been dereddened by $A_V = 1.8$ mag. Error bars are 1σ and are much smaller than the points when not shown. Arrows represent 3σ upper limits to the *Spitzer* IRAC fluxes. The observed SED is compared with the SED of an M3V (open stars). Both V406 Vul and the star of similar brightness and color located 1.″4 north of the system (see "Ref 1" in Figure 2) were unresolved with IRAC. The IRAC measurements are consistent with the sum of the two stellar sources.

We obtained *J*-, *H*-, and K_s-band light curves of MM Vel on 2002 February 22 and 23 with the OSIRIS instrument on the CTIO 4 m telescope. Figure 4 shows the resulting light curves. We have run light curve models using the Eclipsing

Table 5
V406 Vul and "Ref 1" Magnitudes

Object	R (mag)	J (mag)	H (mag)	K_s (mag)
V406 Vul	22.48 ± 0.07	19.50 ± 0.17	19.01 ± 0.16	19.09 ± 0.35
"Ref 1"	23.05 ± 0.04	19.82 ± 0.22	18.85 ± 0.14	18.94 ± 0.31

Note. *JHK* magnitudes listed here were obtained on 2007 October 20, one day after the *Spitzer* observations. *R* mag from Zurita et al. (2002).

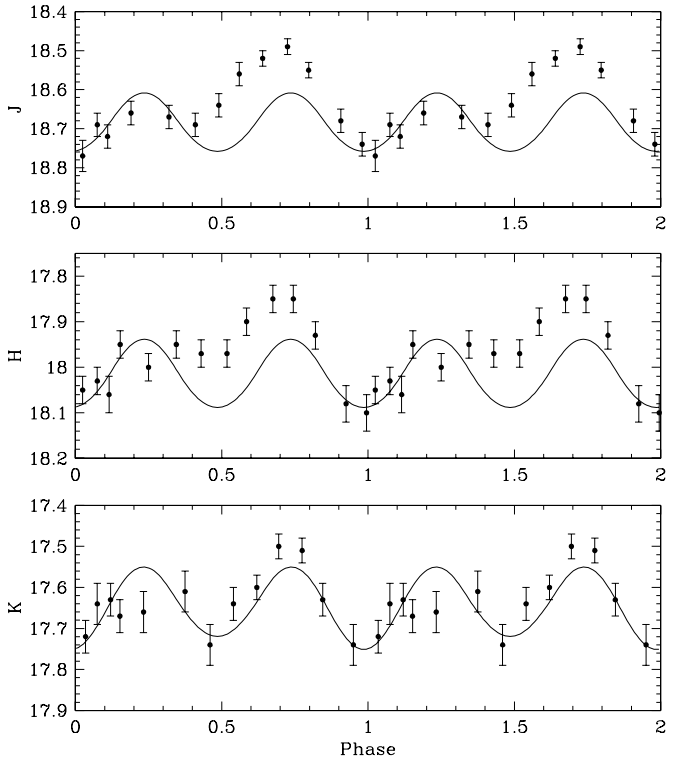

Figure 4. MM Vel *J*-, *H*-, and K_s-band light curves (points) and ELC model light curves (lines). Error bars are 1σ. The data are plotted over two phase cycles for clarity. The light curves show signs of phase-dependent excess emission in the *J* and *H* bands. Such emission probably has an origin in the accretion disk hotspot. The best-fit model has an inclination angle of $i = 58°$.

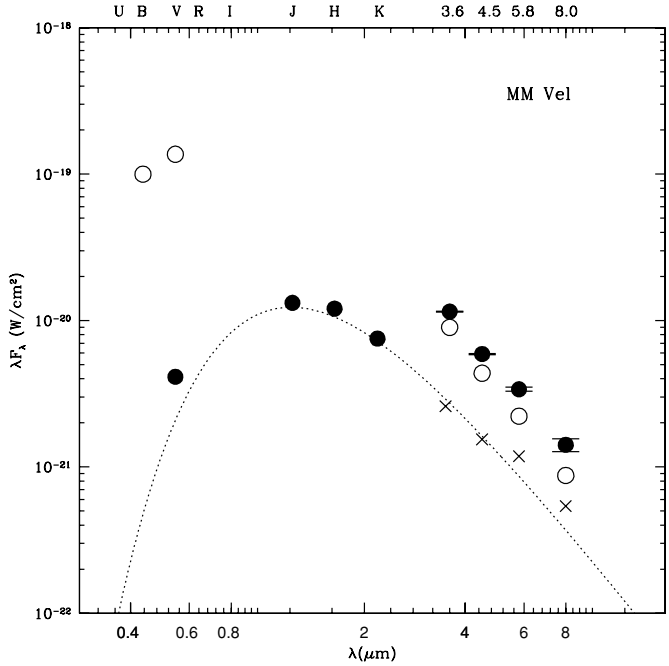

Figure 5. Optical to mid-IR SED for MM Vel (filled circles). The open circles represent the SED for a G7 star. All of the data have been dereddened by $A_V = 0.6$ mag. Error bars are 1σ, and are much smaller than the points when not shown. The observed SED is compared with a 3300 K blackbody representing an M3V (dotted line). MM Vel was unresolved from the G7 star located less than 1.″5 away from the system in the IRAC images. The crosses are a result of subtracting the G star flux from the observed IRAC fluxes. The crosses are consistent with the blackbody, with possible excesses in the two longest IRAC bands.

Light Curve (ELC) code (Orosz & Hauschildt 2000) to model these data. Cursory examination of the data shows that the *J*- and *H*-band light curves are much more highly asymmetric than the *K*-band light curve. Such asymmetries in interacting binaries with accretion disks are usually caused by hotspots on the disks or from irradiation of the secondary star. We focused our light curve modeling on the *K* band since it appears to be dominated by ellipsoidal variations. Because we know very little about this system (including the phasing), we allowed ELC to solve for a best-fit model with mass ratios typical for other BH SXTs: $0.06 \leqslant q \leqslant 0.15$ (see the references to the data in Table 1). The SED, plotted in Figure 5, also suggests a very cool secondary star. Thus, we imposed limits on the secondary star temperature of 3000 K $\leqslant T_{\rm eff} \leqslant$ 4000 K. The best-fit model light curves are plotted in Figure 4 and have the following parameters: $M_1 = 5.3\,M_\odot$, $q = 0.13$, $T_2 = 3100$ K, and $i = 58°$. Clearly, useful limits on the parameters of MM Vel system could be derived given radial velocity data combined with higher quality *JHK* light curves, though it is also clear that a significant accretion component remains and that inclusion of optical light curves into the modeling process would be extremely valuable.

The optical/mid-IR SED for MM Vel is presented in Figure 5. We combined our *Spitzer* data with our ground-based NIR CTIO data and *V*-band data from Hynes et al. (2003). The *B*- and *V*-band data of the nearby G-star are from Masetti (1997) and are plotted as open circles. The IRAC fluxes contained the flux from both MM Vel and the nearby G-star, with the G-star dominating in each of the IRAC bands. In order to derive the MIR fluxes from MM Vel only, we used the StarPet[8] tool to estimate the flux of an unreddened G7 star in each of the IRAC bands (open circles). We then subtracted these fluxes from the IRAC data. The residual fluxes are shown as crosses in Figure 5. We then fit the resulting *VJHK* data set (filled circles) with a 3300 K blackbody assuming $A_V = 0.6$ mag, estimated using the same infrared science archive tool as with V406 Vul above. This blackbody represents an ~M3 secondary star and is slightly hotter than the one derived from our ELC model. To allow for a cooler secondary star, there has to be significantly less extinction than predicted by the online calculator. Unfortunately, given the estimated nature of the fluxes in the IRAC bands, along with the uncertain extinction value and the non-simultaneous nature of the ground-based and space-based data, any conclusions about the presence of a mid-IR excess are difficult to make. That being

[8] http://ssc.spitzer.caltech.edu/warmmission/propkit/pet/starpet/index.html

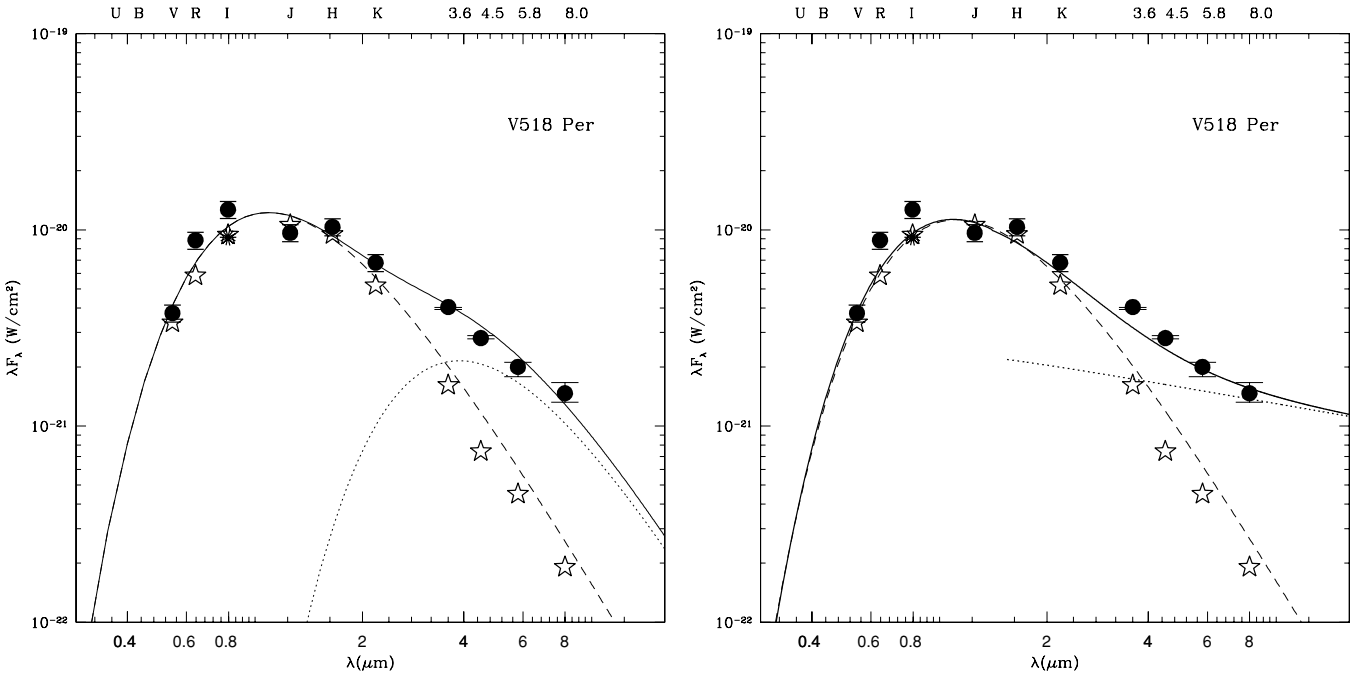

Figure 6. Left: optical to mid-IR SED for V518 Per (filled circles). The optical and infrared data have been dereddened by $A_V = 0.75$ mag. Error bars are 1σ and are much smaller than the points when not shown. The asterisk is from Webb et al. (2000) and shows the system's optical variability during quiescence and the need for simultaneous data sets in order to properly examine SXT SEDs. The observed SED is compared with the SED of an M1V (open stars). The solid line is a composite of a 3650 K (M1V) BB model (dashed line) and a 950 K BB representing a cool dust source (dotted line). Right: data are the same as the left panel. The dashed line again represents the 3650 K BB model as in the left panel, but is now combined with a power law with slope of -0.7 and 1.5 μm cutoff simulating a synchrotron source in the system (dotted line). Both sets of models are consistent with the observed points, however the synchrotron model better describes the trend in the IRAC data.

said, however, there is little evidence for a *strong* mid-IR excess in this system.

3.4. V518 Per

V518 Per was discovered using the Burst and Transient Source Experiment (BATSE) aboard *CGRO* on 1992 August 5 (Paciesas & Briggs 1992), while the V $\sim$ 13 optical counterpart was identified by Castro-Tirado et al. (1993). The X-ray and optical outburst light curves were similar to those of V616 Mon, except that the V518 Per light curves showed a number of "mini-outbursts" following the main eruption (Shrader et al. 1997). Gelino & Harrison (2003) detected *J*-, *H*-, and K_s-band ellipsoidal variations from the system in both 2001 and 2003. The two sets of light curve shapes, amplitudes, and brightnesses were consistent with each other and were modeled simultaneously using WD98, giving an inclination angle of $i = 45^\circ \pm 2^\circ$, and a BH mass of $3.97 \pm 0.95\ M_\odot$. This inclination and BH mass required a 7% contamination in the NIR from an accretion disk (assuming an M1V secondary star).

In 2007, Reynolds et al. (2007) published *K*-band data taken in 1997 September with NIRC on the Keck I telescope. While the *K*-band magnitude was consistent with that reported by Gelino & Harrison (2003), there was no evidence for ellipsoidal variations. This result is identical to that found by Gelino (2001) from data obtained in 1997 January. Since Reynolds et al. (2007) did not attempt to obtain *J*- or *H*-band light curves, their result was based on a *K*-band light curve only. One possible explanation for the lack of *K*-band ellipsoidal variations in 1997 January and September is that V518 Per was undergoing a number of mini-outbursts during 1997 as reported by Iyudin & Haberl (1997) and as can be derived by examining the *RXTE* ASM light curve for this source. These data show that mini-outburst activity was recurring every $\approx$120 days as it slowly declined into quiescence. Additional luminosity from these events could easily compromise the ellipsoidal variations, as well as explain their subsequent visibility once these episodes ended.

Figure 6 presents the de-reddened optical to mid-IR SED of V518 Per. The open stars represent the SED of an M1V, while the filled circles are the observed ground- and space-based data. The fluxes plotted in this figure have been dereddened using $A_V = 0.75$ mag (King et al. 1996 and references therein). While the IRAC and *JHK* data were obtained only three days apart, the optical data are from 2001 (Gelino & Harrison 2003). The single asterisk in the figure is the *I*-band measurement from Webb et al. (2000). See Gelino & Harrison (2003) and references therein for details of the secondary star spectral type determination. The differences between the two *I*-band points show that optical variability exists in the quiescent state and demonstrate that simultaneous data sets are essential to properly examine the SED of this system.

The solid line in the left panel of Figure 6 is the sum of a 3650 K blackbody, representing the M1V secondary (dashed line) and a cool blackbody source with $T_{\rm eff} = 950$ K (dotted line). The right panel shows the same secondary star spectrum (dashed line), but is now combined with a power law ($F_\nu \propto \nu^\alpha$ where $\alpha = -0.7$) that cuts off at 1.5 μm, simulating a synchrotron source in the system (dotted line). This synchrotron model is similar to that proposed for V616 Mon by Gallo et al. (2007). In the synchrotron model, the secondary star accounts for 71% of the flux at *K* and 38% of the flux at 3.5 μm, with the power-law component accounting for the remaining portion of the flux at both wavelengths. Thus, the contamination in the *K* band might be somewhat higher than estimated by Gelino & Harrison (2003). But since we were unable to obtain full NIR light curves at the time of the *Spitzer* observations, we cannot use light curve

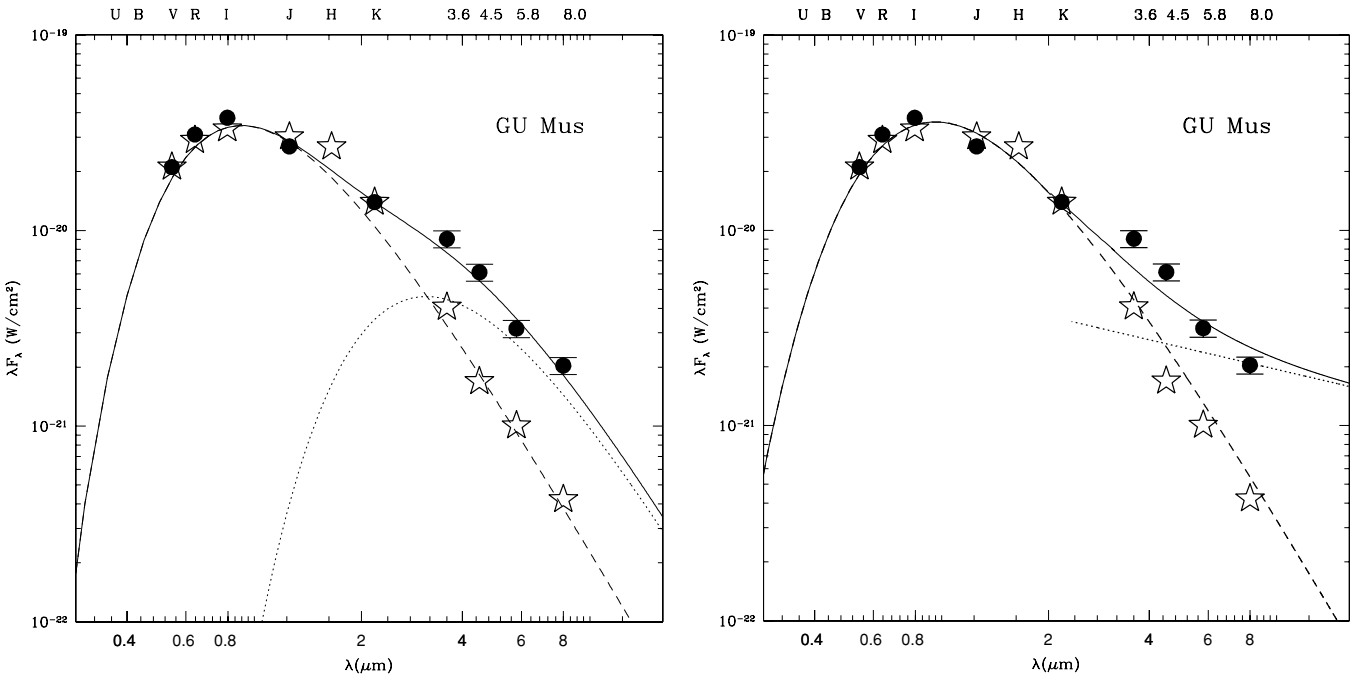

Figure 7. Left: optical to mid-IR SED for GU Mus (filled circles). These data have been dereddened by $A_V = 0.9$ mag. Error bars are 1σ and are much smaller than the points when not shown. The observed SED is compared with the SED of a K4IV (open stars). The solid line is a composite of a 5400 K (G8V) BB model (dashed line) and a 1000 K BB representing a cool dust source (dotted line). This model, while fitting the data, assumes a hotter star than has been spectroscopically determined. Right: data are the same as the left panel. The dashed line now represents a 4700 K (K4IV) BB model, and is combined with a power law with slope of −0.7 and 2.8 μm cutoff simulating a synchrotron source in the system (dotted line).

modeling to examine this result. In addition to explaining the new observations, the natural variability of a synchrotron jet could help explain the changing visibility of the NIR ellipsoidal variations in this system.

3.5. GU Mus

GU Mus was discovered by the *Ginga* and *GRANAT* satellites on 1991 January 9 (Lund et al. 1991; Lund & Brandt 1991). The discovery of the optical counterpart was announced a few days later by Della Valle et al. (1991). Orosz et al. (1996) presented optical spectroscopy of the system from which they derived a mass function of $f(M) = 3.01 \pm 0.15 M_{\odot}$, and estimated that the secondary star had a spectral type of K3/5V. Gelino et al. (2001a) presented *J*- and *K*-band ellipsoidal light curves of this southern hemisphere BH SXT, and found that a K4IV, with $A_V = 0.9$ mag, best fit the observed colors. There have been no further IR studies of the system published. Unfortunately, this means that our ground-based and space-based data sets are far from simultaneous.

The observed, dereddened SED for GU Mus is shown in Figure 7 (filled circles). The *V*-, *R*-, and *I*-band measurements were obtained with the Cassegrain focus CCD Imager on the 0.9 m telescope at CTIO in 2001 March. The open stars in each panel represent the SED for a K4IV. The ground-based and space-based data were taken nearly eight years apart, and due to the variability of the quiescent behavior of SXTs, severely compromises any conclusions generated from the analysis of such a data set. Even so, the IRAC photometry indicates a *strong* mid-IR excess. The left-hand panel of Figure 7 shows a composite model (solid line) comprised of a 5400 K blackbody (∼G8V, dashed line) and a cool source with $T_{\rm eff} = 1000$ K (dotted line). This model, while fitting the observed data, assumes a much hotter secondary star than indicated in previous studies. The right-hand panel combines a K4IV spectrum with a power law ($F_\nu \propto \nu^\alpha$, where $\alpha = -0.7$) that cuts off in the *K* band, simulating a synchrotron source in the system. The power-law model has a secondary star that accounts for all of the flux at *K* and is responsible for 67% of the flux at 3.5μm.

4. SUMMARY AND DISCUSSION

Without sufficient proof, it is dangerous to assume that the NIR ellipsoidal variations which have been detected for a number of BH SXTs are free from contamination. If they are not, then light curve modeling will underestimate the orbital inclination angle and therefore overestimate the primary mass. Emission from an accretion disk, a hotspot, or a jet could all act to dilute the light from the secondary star. In addition, there could be cool dust in these systems that could also contaminate the NIR fluxes. In order to examine this issue, and characterize any non-stellar sources of luminosity, we have combined new and/or existing ground-based optical and NIR data with new mid-IR data from the *Spitzer Space Telescope*. We find evidence for strong mid-IR excesses in two of the five BH SXTs.

Our lack of the detection of significant mid-IR excesses for V406 Vul, MM Vel, and QZ Vul suggests that the infrared luminosities of these systems are dominated by their secondary stars, and thus the amplitudes of their ellipsoidal variations are good measures of their orbital inclinations. However, the presence of mid-IR excesses in V518 Per, GU Mus, and V616 Mon (as previously reported) indicate that this is not always true for BH SXTs. In fact, the existing data set argues that these three sources are quite variable and strictly simultaneous multi-wavelength (including mid-IR) data are required to put useful limits on their orbital inclinations.

As to the nature of the mid-IR excesses, two mechanisms have been proposed: synchrotron jets (Gallo et al. 2007) and

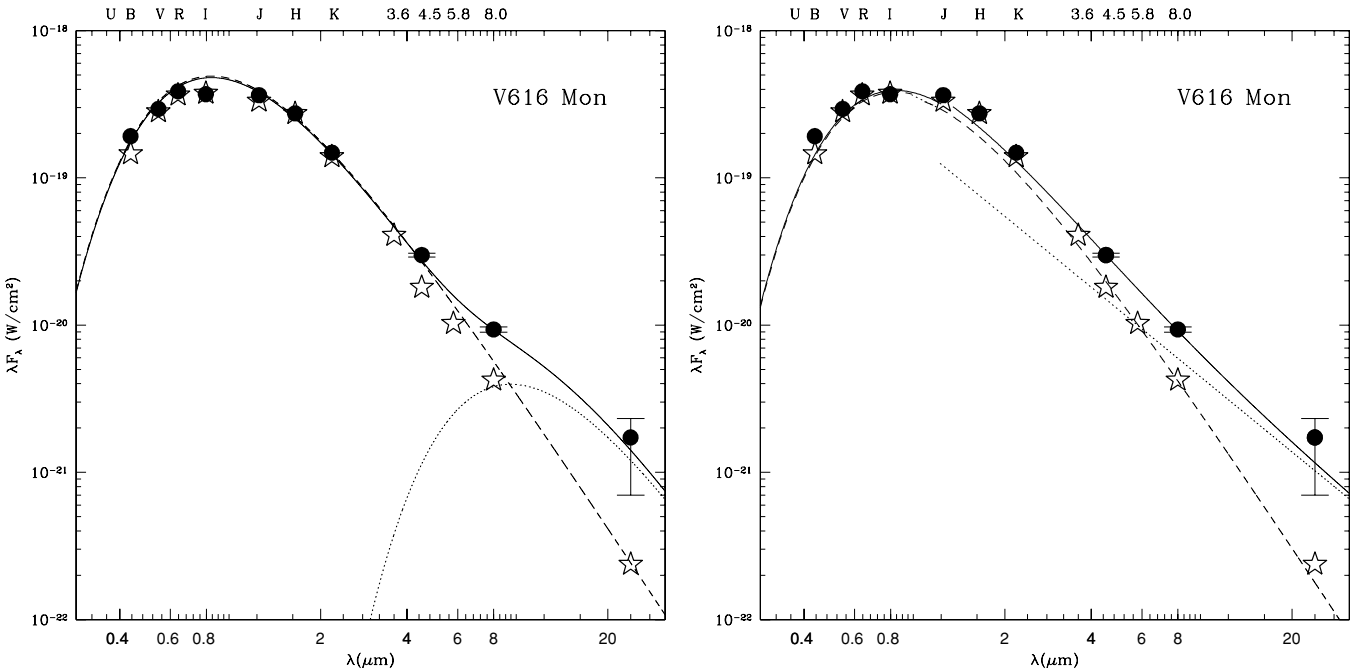

Figure 8. Left: optical to mid-IR SED for V616 Mon (filled circles). These data have been dereddened by $A_V = 1.21$ mag. The *Spitzer* IRAC and MIPS (24μm) data are from Muno & Mauerhan (2006). Error bars are 1σ and are much smaller than the points when not shown. The observed SED is compared with the SED of a K5V (open stars). The solid line is a composite of a 4400 K blackbody model (dashed line) and a 400 K blackbody representing a cool dust source (dotted line). Right: data are the same as the left panel. The dashed line again represents a 4400 K BB model, and is combined with a power law with slope of -0.6 and 0.95 μm cutoff simulating a synchrotron source in the system (dotted line).

dusty circumbinary ("CB") disks (Muno & Mauerhan 2006). Figures 6, 7, and 8 show that both models can be made to be consistent with the observed SEDs of V518 Per, GU Mus, and V616 Mon. However, based on the arguments below, we believe that the synchrotron jet model is the best explanation for the detected emission.

The approximate temperature ($T_{\rm disk}$) of a circumbinary disk of radius ($R_{\rm disk}$) heated by a stellar source can be estimated using Equation (3) from Muno & Mauerhan (2006):

$$T_{\rm disk} \sim \left(\frac{2}{3\pi}\right)^{1/4} \left(\frac{R_*}{R_{\rm disk}}\right)^{3/4} T_*.$$

With radial velocity studies that allow for the derivations of the masses of the components in these systems, we can determine the temperature (T_*) the star needs to be to produce a CB with the observed temperature ($T_{\rm disk}$). This is because we can fix the radius of the star (R_*) using the Roche lobe-filling geometry of the binary. As discussed in Dubus et al. (2004), the innermost stable radius for a CB disk is $1.7a$, where a is the semimajor axis of the binary. For V518 Per, the semimajor axis is $a = 2.54 \pm 0.24\ R_\odot$ (Gelino & Harrison 2003). We will assume the CB disk extends to its minimum allowed radius, $R_{\rm disk} = 4.32\ R_\odot$. Given the solution for the binary parameters of V518 Per listed in Gelino & Harrison (2003), we estimate the secondary star to have a radius of $R_* = 0.53\ R_\odot$. To heat the CB disk to a temperature of $T_{\rm disk} = 950$ K requires the secondary star in V518 Per to have a temperature of $T_* = 6500$ K. This temperature corresponds to a mid-F spectral type, which is inconsistent with both the photometry and spectroscopy of the system. The same calculation for GU Mus (using parameters listed in Gelino et al. 2001a) suggests that the secondary star ($R_* = 1.02\ R_\odot$) would need to have a temperature in excess of 7000 K. While it is true that the solutions for the parameters used to derive R_* for these two systems have some uncertainty, they enter the above equation as a weak power. We would need to increase the stellar radii by more than 50% to get the CB dust to have the observed temperatures, while having secondary stars near their reported spectral types.

Based on the non-linear relation between the radio and X-ray power from low-state BH X-ray binaries, namely that the kinetic power of the jet is much greater than the X-ray luminosity of the accretion flow, Fender et al. (2003) state that since quiescent BH X-ray binaries have relatively low mass accretion rates, all such systems should become jet dominated. Similarly, based on a study of X-ray emission from quiescent BH transients, Pszota et al. (2008) show that quiescent X-ray emission from BH SXTs is more likely to originate from jets, as opposed to accretion processes, and suggest that the X-ray emission from these quiescent systems is dominated by jets. This follows from the fact that at low accretion rates, X-ray emission from jets is proportional to the accretion rate while X-ray emission from hot flows are proportional to the accretion rate squared (Yuan & Cui 2005). Reynolds et al. (2007) rule out the possibility of jets as a contaminating source based on the results of Muno & Mauerhan (2006) for V616 Mon. However, as noted in the Introduction, Gallo et al. (2007) have reanalyzed the Muno & Mauerhan (2006) data and found evidence supporting jet emission based on its multi-wavelength SED. For direct comparison to our results for the other BH SXT systems, we present composite dust and synchrotron models for V616 Mon in Figure 8. The optical and NIR data in this figure are from Gelino et al. (2001b), while the mid-IR *Spitzer* IRAC and MIPS (24 μm) data are from Muno & Mauerhan (2006; with the error bars on the 24 μm flux from Gallo et al. 2007). The dust model combines a 4400 K blackbody with a cool 400 K BB for the dust source. Using the same process as before, we find that the existing secondary star could easily heat a CB disk around V616 Mon to the observed temperature. The right panel of Figure 8 shows the composite

synchrotron model combining the observed secondary star SED with a power law having a spectral index of −0.6 and a cutoff at 0.95 μm. This power law would contribute (weakly) to the NIR fluxes. If true, then varying jet emission could account for the observed variations in the changing infrared light curves of this system.

It is interesting that jet production would appear to be functional all the way down to the very low quiescent luminosities observed for these systems. But Migliari & Fender (2006) conclude that both BH and NS X-ray binaries in low/hard states appear to be able to produce steady jets when their X-ray emission is less than 1% of the Eddington luminosity. Based on ASM light curves taken on the dates of the *Spitzer* data for GU Mus and V518 Per, the systems were not experiencing heightened X-ray activity levels and therefore this jet activity would have to be produced with very low accretion rates.

The suggestion by Gallo et al. (2007) that the MIR excess in V616 Mon might be non-thermal emission from a synchrotron jet can be applied to GU Mus and V518 Per and is completely consistent with our data. Our models indicate that the jet fluxes in both V616 Mon and V518 Per could contaminate their observed NIR fluxes. The changing flux from a jet could account for the varying detection of the ellipsoidal variations in V518 Per noted above and in V616 Mon (Gelino et al. 2001b; Froning & Robinson 2001). Having such emission makes determining the inclination angle using NIR ellipsoidal variations problematic.

If all BH SXTs exhibit identical behavior, then the six systems discussed here (including V616 Mon) suggest that such emission has a $\approx$ 50% duty cycle. These six systems cover nearly the entire range of orbital periods and semimajor axes observed for BH SXTs. In that case, it would simply be a coincidence that half of the systems show evidence for jets. Clearly, further optical, infrared, and radio monitoring of all quiescent BH SXTs is required to fully decipher both the nature, and duty cycle of these excesses.

In this study, we have combined ground-based optical and NIR data with *Spitzer* IRAC data for five BH SXTs, and found evidence for jets in these quiescent systems. Assuming the excess emission found is due to jets, multi-epoch MIR studies can be used to monitor jet activity in SXTs as well as the frequency of the jet turnover. We do not see any evidence for needing dust around these systems in order to explain their MIR excesses.

Facilities: Spitzer (IRAC), Hale Telescope (WIRC), ARC (SPIcam), Blanco (OSIRIS).

REFERENCES

Bildsten, L., & Rutledge, R. 2000, ApJ, 541, 908
Callanan, P., et al. 1995, ApJ, 441, 786
Cannizzo, J. 2000, ApJ, 534, L35
Cantrell, A., et al. 2010, ApJ, 710, 1127
Castro-Tirado, A., Pavlenko, E., Shlyapniko, A., Bandt, S., Lund, N., & Ortiz, J. 1993, A&A, 276, L37
Charles, P., & Coe, M. 2006, in Compact Stellar X-Ray Sources, Cambridge Astrophysics Series 39, ed. W. H. G. Lewin & M. van der Klis (Cambridge: Cambridge Univ. Press), 215
Charles, P., Kidger, M., Pavlenko, E., Prokofieva, V., & Callanan, P. 1991, MNRAS, 249, 567
Della Valle, M., & Benetti, S. 1993, IAU Circ., 5890, 2
Della Valle, M., Jarvis, B., & West, R. 1991, IAU Circ., 5165, 2
Della Valle, M., Benetti, S., Cappellaro, E., & Wheeler, C. 1997, A&A, 318, 179
Dubus, G., Campbell, R., Kern, B., Tamm, R. E., & Spruit, H. C. 2004, MNRAS, 349, 869
Fazio, G., et al. 2004, ApJS, 154, 10
Fender, R., Gallo, E., & Jonker, J. 2003, MNRAS, 343, 99
Filippenko, A., & Chornock, R. 2001, IAU Circ., 7644, 2
Flaherty, K. M., Pipher, J. L., Megeath, S. T., Winston, E. M., Gutermuth, R. A., Muzerolle, J., Allen, L. E., & Fazio, G. G. 2007, ApJ, 663, 1069
Froning, C., & Robinson, E. 2001, AJ, 121, 2212
Gallo, E., Migliari, S., Markoff, S., Tomsick, J., Bailyn, C., Berta, S., Fender, R., & Miller-Jones, J. 2007, ApJ, 670, 600
Garcia, M., McClintock, J., Narayan, R., Callanan, P., Barret, D., & Murray, S. 2001, ApJ, 553, L47
Garnavich, P., & Quinn, J. 2000, IAU Circ., 7388, 3
Gelino, D., & Harrison, T. 2003, ApJ, 599, 1254
Gelino, D., Harrison, T., & McNamara, B. 2001a, AJ, 122, 971
Gelino, D., Harrison, T., & Orosz, J. 2001b, AJ, 122, 2668
Gelino, D. M. 2001, PhD thesis, New Mexico State Univ.
Gelino, D. M. 2002, BAAS, 34, 654
Harmon, B., Zhang, S., Fishman, G., & Paciesas, W. 1993, IAU Circ., 5864, 2
Harrison, T. E., Howell, S., Szkody, P., & Cordova, F. 2007, AJ, 133, 162
Hjellming, R., & Rupen, M. 1995, Nature, 375, 464
Hjellming, R., et al. 1988, ApJ, 335, L75
Hynes, R., Charles, P., Casares, J., Haswell, C., Zurita, C., & Shahbaz, T. 2003, MNRAS, 340, 447
Hynes, R., Robinson, E., & Bitner, M. 2005, ApJ, 630, 405
Iyudin, A., & Haberl, F. 1997, IAU Circ., 6738, 1
Kaniovsky, A., Borozdin, K., & Sunyaev, R. 1993, IAU Circ., 5878, 1
King, N. L., Harrison, T. E., & McNamara, B. J. 1996, AJ, 111, 1675
Lapshov, I., Sazonov, S., & Sunyaev, R. 1993, IAU Circ., 5864, 1
Lasota, J. 2008, New Astron., 51, 752
Lund, N., Brandt, S., Makino, F., McNaught, R., Jones, A., & West, R. 1991, IAU Circ., 5161, 1
Lund, H., & Brandt, S. 1991, IAU Circ., 5161, 1
Makino, F., Wagner, R., Henden, A., Bertram, R., & Starrfield, S. 1988, IAU Circ., 4600, 2
Masetti, N. 1997, PhD thesis, University La Sapienza, Rome, Italy
Migliari, S., & Fender, R. 2006, MNRAS, 366, 79
Migliari, S., Tomsick, J., Maccarone, T., Gallo, E., Fender, R., Nelemans, G., & Russell, D. 2006, ApJ, 643, 41
Muno, M., & Mauerhan, J. 2006, ApJ, 648, L135
Orosz, J., Bailyn, C., McClintock, J., & Remillard, R. 1996, ApJ, 468, 380
Orosz, J.A., & Hauschildt, P.H. 2000, A&A, 364, 265
Owen, F., Balonek, T., Dickey, J., Terzian, Y., & Gottesman, S. 1976, ApJ, 203, L15
Paciesas, W., & Briggs, M. 1992, IAU Circ., 5580, 1
Pszota, G., Zhang, H., Yuan, F., & Cui, W. 2008, MNRAS, 389, 423
Reynolds, M., Callanan, P., & Filippenko, A. 2007, MNRAS, 374, 657
Russell, D., Fender, R., Hynes, R., Brocksopp, C., Homan, J., Jonker, P., & Buxton, M. 2006, MNRAS, 371, 1334
Shahbaz, T., van der Hooft, F., Charles, P., Casares, J., & van Paradijs, J. 1996, MNRAS, 282, L47
Shahbaz, T., et al. 2003, MNRAS, 346, 1116
Shrader, C., Wagner, R., Charles, P., Harlaftis, E., & Naylor, T. 1997, ApJ, 487, 858
Tsunemi, H., Kitamoto, S., Okamura, S., & Roussel-Dupre, D. 1989, ApJ, 337, L81
Webb, N., Naylor, T., Ioannou, Z., Charles, P., & Shahbaz, T. 2000, MNRAS, 317, 528
Werner, M., et al. 2004, ApJS, 154, 1
Wijnands, R. 2005, in Progress in Neutron Star Research, ed. A. P. Wass (Hauppauge, NY: Nova Science)
Wilson, J., et al. 2003, Proc. SPIE, 4841, 451
Wood, A., Smith, D., Marshall, F., & Swank, J. 1999, IAU Circ., 7274, 1
Yuan, F., & Cui, W. 2005, ApJ, 629, 408
Zurita, C., et al. 2002, MNRAS, 334, 999